SHORT COMMUNICATION

I^{5}M: 3D widefield light microscopy with better than 100 nm axial resolution

M. G. L. GUSTAFSSON,* D. A. AGARD*† & J. W. SEDAT*

*Department of Biochemistry and Biophysics, University of California, San Francisco, CA 94143-0448, U.S.A.

†Howard Hughes Medical Institute, University of California, San Francisco, CA 94143-0448, U.S.A.

Summary

Sevenfold improved axial resolution has been achieved in three-dimensional widefield fluorescence microscopy, using a novel interferometric technique in which the sample is observed and/or illuminated from both sides simultaneously using two opposing objective lenses. Separate interference effects in the excitation light and the emitted light give access to higher resolution axial information about the sample than can be reached by conventional widefield or confocal microscopes. Here we report the experimental verification of this resolution performance on complex biological samples.

Introduction

The light microscope remains a ubiquitous and irreplaceable research tool for modern biology. Unlike any other microscope it allows: (i) samples to be studied *in vivo* or in their native hydrated environments, (ii) highly specific labelling of multiple components, and (iii) detailed internal structures to be viewed in three dimensions. Its dominant weakness is its limited resolution, particularly in the axial, or focus, direction. Computational deconvolution (Agard *et al.*, 1989) and confocal (Pawley, 1990) techniques have improved the resolution both laterally and, especially, axially, but still leave the axial resolution several times worse than the lateral. The wide popularity of these techniques over the last decade attests to the impact that resolution improvements in optical microscopy can have on biology.

Correspondence to: Dr D. A. Agard. Tel: + 1 415 476 2521; fax: + 1 415 476 1902; e-mail: agard@msg.ucsf.edu

The resolving power of the optical microscope is fundamentally limited by the wavelength of light. As was understood by Ernst Abbe more than a century ago (Abbe, 1873), resolution limits become less stringent the larger the set of angles over which the objective lens gathers light – indeed the primary figure of merit of an objective lens, its numerical aperture (NA), is simply a measure of this angle. Since lens design is by now a mature technology, the light collecting angle of commercially available objective lenses is close to its practical maximum, with little if any room for further improvement. However, there exists an equally large set of easily accessible light collecting angles on the 'back' side of the sample slide, which conventional microscopes do not make use of. We have developed a new microscope design that does utilize this light, using a second objective lens on the back side of the sample, thereby achieving dramatically improved resolution in the difficult axial direction (Gustafsson *et al.*, 1995, 1996). Here we report the first biological images from this system and the experimental verification of the resolution gain.

In the new mode we call 'image interference microscopy', I^{2}M, a fluorescent sample is mounted between two opposing objective lenses, each of which is focused on the same focal plane within the sample and forms a magnified image of this plane. These two images are combined by a beamsplitter and superposed on a single CCD camera (Fig. 1A). The optical path lengths of the two image beams are adjusted to be equal, causing the two beams of light from each fluorescent molecule to interfere with each other on the camera; the interference pattern contains high resolution information about the axial position of the molecule in question. If, instead or in addition, the excitation light is made to traverse the two paths and impinge on the sample
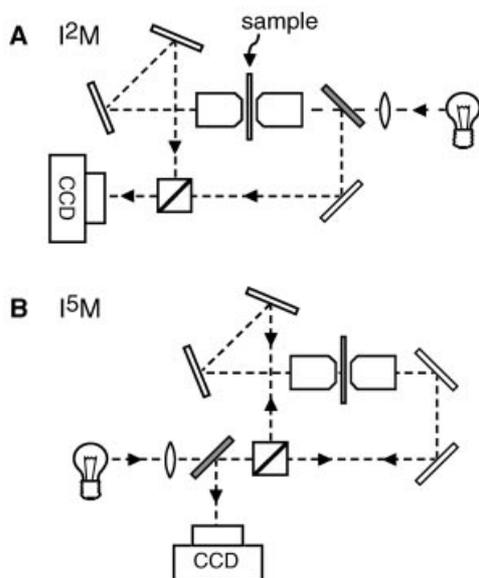
Fig. 1. Concept of I^2M, where the sample is observed from both sides (A), and I^5M, where it is also illuminated from both sides (B).

through both lenses (Fig. 1B), an axially varying illumination intensity is created through interference. In a manner similar to standing wave microscopy (Bailey *et al.*, 1993; Lanni *et al.*, 1993), this non-uniform excitation field modulates the pattern of emitted light and thereby encodes high-resolution axial information. We refer to this as 'incoherent interference illumination', I^3, since it uses an extended, spatially incoherent light source such as a standard arc lamp. The two kinds of interference are independent and can with advantage be used at the same time (I^5M).

In either mode, acquisition proceeds just as in normal computational deconvolution microscopy (Agard *et al.*, 1989): a focal series of images are recorded, with the sample moved slightly between each image to change the plane of focus. The resulting data set is computationally processed (deconvolved) to remove out-of-focus blur and create a 3D reconstruction of the sample.

Theoretical background

The information gathering properties of any linear, translation-invariant imaging system can be completely described by its 'optical transfer function' (OTF), a function in reciprocal space (also called Fourier space, the space of spatial frequencies) which describes how strongly, and with what phase shift, each spatial frequency component of the sample structure is transferred into the recorded image data. The resolution limits on an optical system, such as a fluorescence microscope, manifest themselves through the fact that the OTF is non-zero only over a finite region (its 'support'), which thus defines the set of spatial frequencies about which the image data contain any information at all. Within the OTF support, the sample information can in principle be restored completely through a simple computational rescaling ('linear inverse filtering'), but all information about spatial frequency components outside of the OTF support has been irretrievably lost. The goal of improving microscope resolution thus translates into a goal of enlarging the OTF support.

The theoretical OTF support of a conventional widefield fluorescence microscope has a torus-like shape (Fig. 2A) (Streibl, 1985; Gustafsson *et al.*, 1995). Its axial extent (given by $[1-\cos(\alpha)]n/\lambda$, where α is the light-gathering half-angle of the objective lens, λ is the wavelength of the emitted light and n the refractive index of the sample medium) is several times smaller than its lateral extent (given by $2\sin(\alpha)n/\lambda$), illustrating the fact that the axial resolution is worse than the lateral resolution. For the I^2M mode, the inter-beam interference effects are expected to
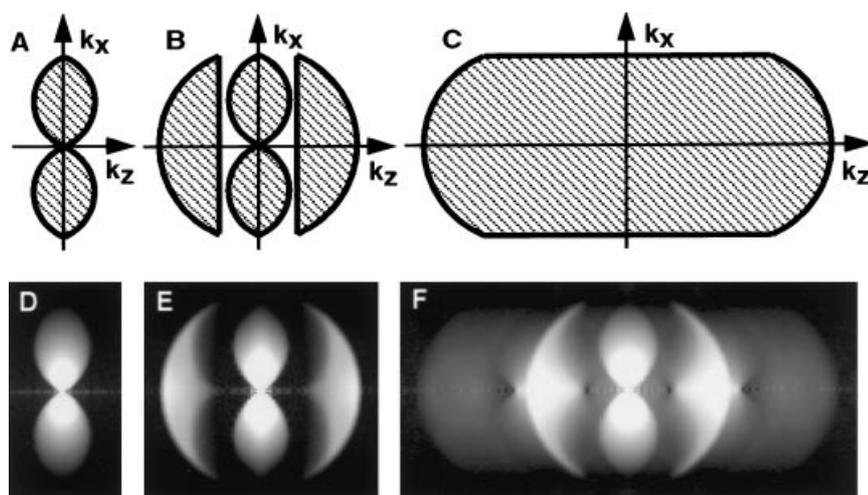

Fig. 2. Theoretically expected OTF supports (A–C) and experimentally measured OTFs (D–E) for conventional microscopy (A,D), I^2M (B,E) and I^5M (C,F). OTFs shown in D–F are displayed using a nonlinear grey scale to show weak regions clearly.

generate two axial side bands in the OTF (Fig. 2B) (Gustafsson *et al.*, 1995). These side bands correspond to new information that cannot be accessed by a conventional microscope. However, the intervening informationless gaps are a drawback – an OTF without such gaps would make deconvolution much more straightforward. As we shall see, I^5M removes this drawback. The effective OTF of the I^5M mode is given by a convolution of the I^2M OTF with the Fourier transform of the illumination structure, which itself consists of three bands (Gustafsson *et al.*, 1995). The resulting nine bands overlap to form an OTF support without gaps, and which extends even further than the I^2M OTF (Fig. 2C). In fact, the axial resolution information that can be accessed by I^5M is slightly more than twice as high as with I^2M, approximately 3·5 times higher than with confocal microscopy, and about seven times higher than with conventional widefield microscopy.

Materials and methods

Microscope system

The prototype microscope system used a pair of matched Nikon PlanApo 100× NA 1·4 oil immersion objective lenses and a Photometrics (Tucson, AZ) cooled CCD camera. The excitation light was s-polarised using a crude tangential polariser (Oriel, Stratford, CT). Superposition of the two image beams was maintained by controlling the XYZ position of one of the objective lenses, using electrostrictive actuators operated in closed loop with capacitive position sensors. The closed loop setpoints were periodically recalibrated by analysing the image of an external point source projected onto the CCD through the two objectives. Similarly, the equality of the two beam paths was maintained by controlling the position of a stage carrying two mirrors (the right side mirrors in Fig. 1), with the set point recalibrated using interference fringes on the CCD from an infrared laser beam reflected off a dichroic mirror at the base of each objective lens. Recalibration of all four degrees of freedom required only 1·7 s and could thus be automatically interspersed during each data set without significant time penalty. This system maintains alignment to better than 10 nm for several hours, more than enough since each data set takes only 10–20 min to acquire. A more detailed description of the microscope hardware will be published elsewhere.

I^5M image data were processed with a truncated inverse filter (equal to the inverse OTF where the OTF magnitude is above a threshold and zero elsewhere, multiplied by an apodization function), followed by a few iterations of the Jannson–van Cittert method which imposes the positivity constraint (Agard *et al.*, 1989). Comparison conventional microscopy data were processed only with modifed Jannson–van Cittert iterations – linear inverse filtering is not helpful

on such data owing to the 'missing cone' of information in reciprocal space.

Resolution characterization

One hundred and sixty images of a 50 nm diameter fluorescent bead (Molecular Probes, Eugene, OR) were acquired at 36·6 nm focus intervals. The 3D Fourier transform of the resulting 3D data set was rotationally averaged to minimize noise (since the OTF is expected to be rotationally symmetric around the optical axis). Comparison data for conventional microscopy were acquired by blocking one of the objective lenses with a shutter.

Biological test samples

PtK2 tissue culture cells were grown on cover slips, extracted for 20 s in microtubule stabilizing buffer (80 mM PIPES pH 6·8, 1 mM $MgCl_2$, 5 mM EGTA, 0·1% Triton X-100 detergent), fixed by adding glutaraldehyde to 0·5% for 10 min, reacted with 0·1% sodium borohydride for 7 min to quench autofluorescence, then labelled with mouse anti-tubulin antibodies and rhodamine-conjugated antimouse secondary antibodies (A. Desai, personal communication). To optimize the optical properties of the sample, the specimen was exchanged into an index-of-refraction-matched mounting medium composed of ≈ 53% benzyl alcohol, 45% glycerol and 2% N-propyl gallate by weight, adjusted to have the same refractive index (1·513) as the immersion oil we had determined to be optimal for the objective lenses. One hundred and sixty optical sections were acquired at 36·6 nm focus intervals.

Results

Quantitative resolution characterization

The OTF of an actual microscope can be determined experimentally by measuring the point spread function (PSF), the characteristic blurred image formed when the sample is a point source: the PSF and OTF are each other's Fourier transforms. Ideal point sources do not exist, but an excellent approximation is available in the form of minute fluorescent beads. Measured OTFs of our prototype microscope in the conventional, I^2M and I^5M modes are in excellent agreement with theory and clearly demonstrate the presence and shape of the I^2M side bands and the superior OTF support of I^5M (Gustafsson *et al.*, 1996). Recent system improvements have minimized the gap in the I^2M OTF and improved the uniformity of the I^5M OTF within its support (Fig. 2D–F).

In the raw image data, the new information manifests itself as an interference pattern containing a sharp central peak and a series of side lobes, seen most clearly with a
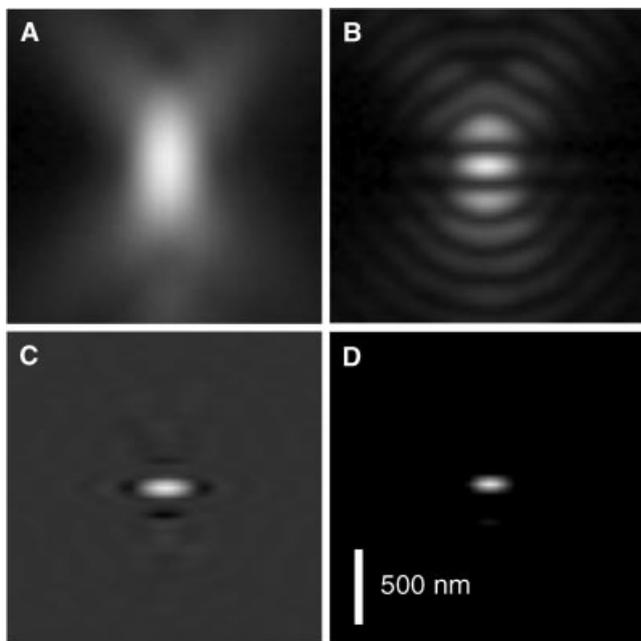
Fig. 3. Side (XZ) views of a 50-nm diameter fluorescent bead (= measured PSFs): (A) conventional widefield microscopy, (B) I^{5}M (raw data), (C) I^{5}M with a linear inverse filter, (D) I^{5}M with a linear inverse filter followed by iterative deconvolution.

point source sample (Fig. 3A,B). Because there are no gaps in the I^{5}M OTF, simple computer processing with a linear inverse filter is sufficient to remove the real space side lobes, leaving the sharp image plus only a slight ringing (Fig. 3C). Because such a filter is a linear operation it will have the same efficiency at removing side lobes on a complex sample as on this point object. The residual ringing can be largely suppressed by imposing the obvious *a priori* constraint that the dye density cannot be negative anywhere, and iterating (Agard *et al.*, 1989) towards a self-consistent solution (Fig. 3D). The resulting reconstruction of the point object has a full width at half maximum (FWHM) of ≈ 70 nm in the axial direction, a dramatic improvement compared to the 650–350 nm achieved by conventional widefield or confocal microscopes.

Biological test samples

To create a more realistic biological test sample, we immunofluorescently labelled the microtubule cytoskeleton of PtK2 tissue culture cells. The diameter of each microtubule is known to be ≈ 25 nm when bare and should remain well below the microscope resolution even after addition of the antibodies. (They are not perfect tubular test objects, however, in that the fluorescence intensity varies somewhat along each microtubule due to varying antibody coverage.) A lateral (XY) view of a deconvolved and reprojected I^{5}M data set of this sample compared to a
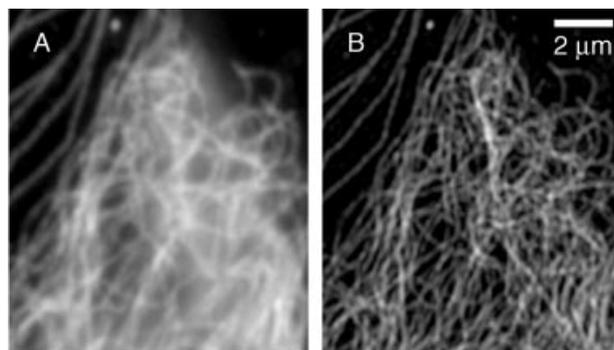

Fig. 4. XY views of fluorescently labelled microtubules in PtK2 tissue culture cells: (A) Conventional microscopy (single section), (B) I^{5}M using a linear inverse filter followed by iterative deconvolution (reprojected).

conventional microscope image of the same region (Fig. 4) demonstrates the well-known suppression of out-of-focus blur by deconvolution. This lateral performance is not substantially different from what can be achieved with conventional deconvolution or confocal microscopes – the strength of the I^{5}M technique lies in the axial direction. Side (XZ) views of the same cell show that while little axial information about this dense sample is detectable in the conventional microscope raw data (Fig. 5A), the I^{5}M raw
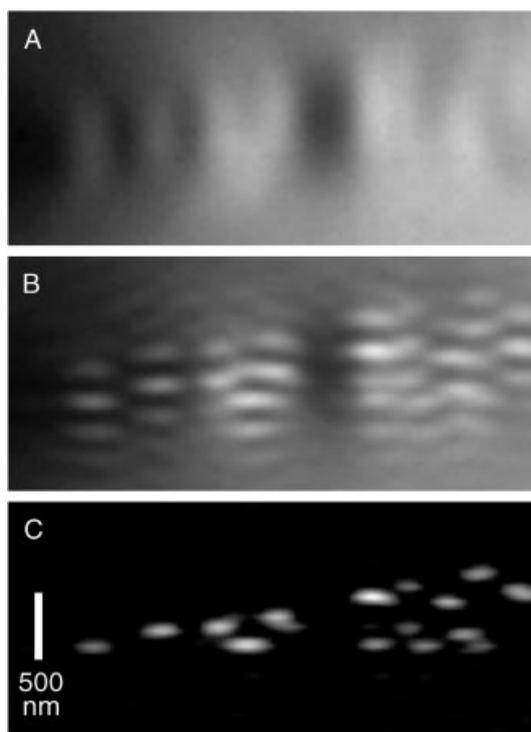

Fig. 5. Side (XZ) views of a portion of the same cell as in Fig. 4: (A) conventional microscopy, (B) I^{5}M (raw data), (C) I^{5}M after deconvolution. Bright spots in (C) correspond to cross-sections of individual microtubules.
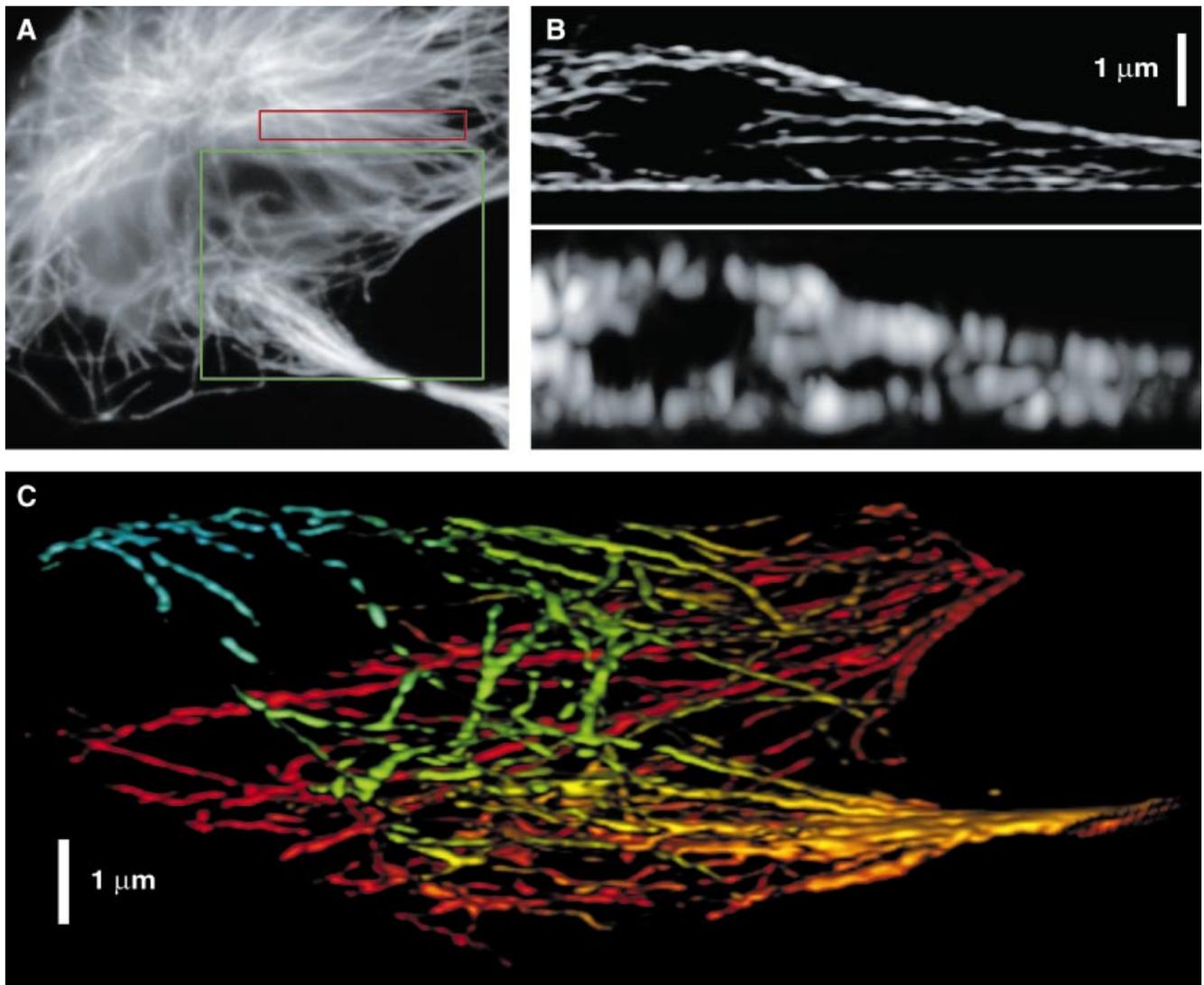
Fig. 6. Microtubules in a PtK2 cell which has recently divided and is still joined to its sister cell by the midbody. (A) Conventional microscope, single section. The red and green boxes indicate the areas rendered in (B) and (C), respectively. (B) Comparison of deconvolved side (XZ) views using I^{5}M (top) and conventional (bottom) microscopy. Maximum intensity projections through a $1\cdot2\,\mu$m wide slice of the cell. Individual microtubules that are obscured by Z blurring in the conventional microscope are clearly distinguished with the I^{5}M due to its superior axial resolution. (C) 3D view of I^{5}M reconstruction. Note the nuclear cavity at left and the dense bundle of microtubules radiating from the midbody at lower right. (Volume rendered by letting the opacity and brightness of each voxel be determined, respectively, by the local fluorescence intensity at that point and by the intensity gradient direction relative to a 'light source', and letting the colour hue vary from red to blue with increasing distance from the substrate on which the cell was grown. View angle 70° off axis.)

data contain considerably more structure (Fig. 5B). That structure, while not easily interpretable to the eye, carries the information necessary to allow the processing algorithm to generate a high-resolution reconstruction where the individual microtubules are resolved (Fig. 5C). As expected, each microtubule appears as a rope-like object in the reconstructed 3D data set, and can be traced through the cell (Fig. 6). The axial FWHM of each microtubule image is

70–90 nm, in good agreement with expectations and in sharp contrast to the performance of conventional techniques (Fig. 6B). Since this is not a confocal technique there is no need for XY scanning; large areas can be imaged simultaneously, limited only by the size of the CCD (today typically 1024×1024 pixels). As an example, the original data set used for Fig. 6(C) covers approximately four times the area shown in the figure.

Discussion

Relation to existing techniques

The I^nM modes of microscopy described here share some aspects with other recent techniques, in particular standing wave fluorescence microscopy (SWFM) (Bailey et al., 1993; Lanni et al., 1993), 4Pi confocal microscopy (Hell & Stelzer, 1992, Hell et al., 1997; Schrader et al., 1998), and multiple telescope interference imaging in astronomy (Reasenberg, 1998). In SWFM, a standing wave of excitation light is created in the sample by interference of two counter-propagating laser beams. By varying the angle of the laser beams one can achieve an effective OTF similar to that of I^3M. Like both I^3M and I^2M, the SWFM OTF suffers from a gap problem which complicates deconvolution, while the I^5M OTF contains no such gaps.

4Pi confocal microscopy (and its multiphoton derivatives) can be thought of as a scanning equivalent of the I^nM techniques: two opposing objective lenses are used to carry excitation and/or emission light in both directions; interference effects carry new spatial information; and computational deconvolution is necessary to remove side lobes. In fact, the most powerful 'type C' mode of 4Pi confocal microscopy reaches the same theoretical axial resolution limit as does I^5M. However, 4Pi confocal is a sample scanning technique and acquires only a single data voxel at a time, after which the sample is moved to the next XY position. In contrast, our new modes are true image-forming widefield microscopies where a CCD camera can be used to acquire an entire XY plane simultaneously without need for scanning, allowing much higher speeds and/or larger image areas. We acquire a $512 \times 512 \times 160$ pixel data set in 10–20 min; to acquire a data set of that size using a typical 4Pi confocal microscope with a pixel dwell time of 2 ms (Schrader et al., 1998) would take almost 24 hours.

Neither SWFM nor 4Pi confocal microscopy share the signature element of I^2M and I^5M, that whole images formed through separate apertures are combined interferometrically. To our knowledge, the only existing technology that does is in the field of astronomy, where interferometric combination of multiple optical telescopes is an area of much recent excitement (Raesenberg, 1998).

Practical limitations

The one engineering challenge of the I^nM techniques is to achieve and maintain alignment of the interferometric loop without significant demands on time or user effort. We do not believe this to be a major hurdle – our prototype already incorporates an automatic alignment control system that maintains nanometre-scale alignment over several hours without user input. A more fundamental limitation relates to the sample itself: any technology, such as I^nM, SWFM or 4Pi confocal, that accesses focal planes within the sample from both sides is inherently limited to a class of reasonably thin and transparent samples. In particular, the interference effects on which they are based can be perturbed by refractive index variations within the sample. While this problem can be diminished by sample preparation protocols specifically aimed at optical homogeneity and by deconvolution algorithms that automatically adapt to spatially varying phase errors, all these techniques will eventually face some upper limit to sample thickness. This limit has yet to be determined in practice, but a crude estimate can be made from the data in Fig. 6. In that data set, where the mounting medium was index-matched to the immersion oil and not specifically to the sample structures, we see no measurable phase error ($< 10°$) through more than $3\,\mu m$ of dense nuclear material (Fig. 6). We therefore have good hope that several tens of micrometres should be within reach under favourable circumstances, opening up a large class of cellular biology questions to investigation by high resolution 3D fluorescence microscopy.

Acknowledgements

References

Abbe, E. (1873) Beiträge zür Theorie des Mikroskops und der mikroskopischen Wahrnehmung. *Arkiv Mikroskopische Anat.* **9**, 413–468.

Agard, D.A., Hiraoka, Y., Shaw, P. & Sedat, J.W. (1989) Fluorescence microscopy in three dimensions. *Methods Cell Biol.* **30**, 353–377.

Bailey, B., Farkas, D.L., Taylor, D.L. & Lanni, F. (1993) Enhancement of axial resolution in fluorescence microscopy by standing-wave excitation. *Nature*, **366**, 44–48.

Gustafsson, M.G.L., Agard, D.A. & Sedat, J.W. (1995) Sevenfold improvement of axial resolution in 3D widefield microscopy using two objective lenses. *Proc. SPIE*, **2412**, 147–156.

Gustafsson, M.G.L., Agard, D.A. & Sedat, J.W. (1996) 3D widefield microscopy with two objective lenses: experimental verification of improved axial resolution. *Proc. SPIE*, **2655**, 62–66.

Hell, S.W., Schrader, M. & van der Voort, H.T.M. (1997) Far-field fluorescence microscopy with three-dimensional resolution in the 100-nm range. *J. Microsc.* **187**, 1–7.

Hell, S. & Stelzer, E.H.K. (1992) Properties of a 4Pi confocal fluorescence microscope. *J. Opt. Soc. Am. A*, **9**, 2159–2166.

Lanni, F., Bailey, B., Farkas, D.L. & Taylor, D.L. (1993) Excitation

field synthesis as a means for obtaining enhanced axial resolution in fluorescence microscopes. *Bioimaging*, **1**, 187–196.

Pawley, J.B., ed. (1990) *Handbook of Biological Confocal Microscopy.* Plenum Press, New York.

Reasenberg, R.D., ed. (1998) Astronomical interferometry. *Proc. SPIE,* **3350**, entire volume.

Schrader, M., Hell, S.W. & van der Voort, H.T.M. (1998) Three-dimensional super-resolution with a 4Pi-confocal microscope using image restoration. *J. Appl. Phys.* **84**, 4033–4042.

Streibl, N. (1985) Three-dimensional imaging by a microscope. *J. Opt. Soc. Am. A*, **2**, 121–127.